Computer simulation of ion conductance in membrane channels

Matthew Hoyles,[1,2] Serdar Kuyucak,[2] and Shin-Ho Chung[1]
[1]*Protein Dynamics Unit, Department of Chemistry, Australian National University, Canberra, Australian Capital Territory 0200, Australia*
[2]*Department of Theoretical Physics, Research School of Physical Sciences, Australian National University, Canberra, Australian Capital Territory 0200, Australia*
(Received 20 February 1998)

We present a method for calculation of electric forces in biological channels, which facilitates microscopic modeling of ion transport in channels using computer simulation. The method is based on solving Poisson's equation on a grid and storing the electric potential and field for various configurations in a table. During simulations, the potential and field at any point are calculated by interpolating between table entries rather than solving Poisson's equation. This speeds up computer simulations by orders of magnitude with minimal loss in accuracy. With this method, one can run simulations long enough to determine the channel conductance, which can be compared directly with experimental data. Since conductance is the most important observable quantity in description of membrane channels, this method will be very useful in future simulation studies of channels. [S1063-651X(98)11209-6]

PACS number(s): 87.22.Fy

I. INTRODUCTION

Study of ion transport in biological membrane channels is one of the most challenging problems in theoretical biophysics [1]. The dimensions of channels (a few angstroms in the narrow region) and the number of ions involved (a few at most at a given time) are such that macroscopic methods are not expected to provide a physical basis for understanding of ion transport in channels. On the other hand, a completely microscopic model based on molecular dynamics (MD) simulation of all the ions and water molecules in and in the vicinity of the channel is not feasible either. Even on the fastest supercomputer currently available, such a simulation would take years of computer time. Brownian dynamics (BD), where ionic motion is treated microscopically but water as bulk, offers a workable compromise between the two extremes and could provide useful insights into the ion transport problem in membrane channels [2].

Past theoretical studies of ion channels have focused mostly on artificial membrane channels such as gramicidin A, which can be modeled as a narrow cylindirical tube with radius 2 Å. Due to their simplicity and small volume, these channels have been studied in great detail using a variety of macroscopic [1] and microscopic theories [2,3]. In contrast, actual biological channels have more complicated shapes and much larger volumes and therefore their modeling is more involved. Typically, biological channels have wide vestibular openings and follow a catenary shape down to a narrow neck region [4]. This geometry poses a serious problem for calculation of electric forces acting on an ion in the channel. Because proteins forming the channels have a low dielectric constant (2) compared to water (80) in which ions move, the channel boundary plays a significant role in determining the electric forces. While numerical solution of Poisson's equation for arbitrary channel boundaries can be readily achieved using iterative techniques [5,6], this is too time consuming to be of any practical use in computer simulations. The alternative, analytical solutions of Poisson's equation can be achieved only in a limited number of coordinate systems. Of these, the toroidal coordinates come closest to forming a realistic channel, that is, a constant surface generates a torus shape [7]. Though the curvature of an actual channel boundary is opposite to that of a torus, the potential profiles obtained for the two boundaries are quite similar and thus the torus could serve as a useful model for ion channels. With the speed gained from analytical solutions, it is possible to carry out BD simulations of ions in vestibular channels long enough to learn about their dynamical behavior [8]. Unfortunately, the analytical solutions of Poisson's equation in toroidal coordinates are rather complicated, requiring still a substantial numerical effort for calculation of electric forces. Thus the gain in speed is not sufficient to obtain the conductance of a model channel. As the conductance provides a direct link between simulations and experiments, its computation is essential for purposes of model building.

Rather than waiting for even faster computers, we propose a different strategy for calculation of electric forces that exploits the huge storage capacity of supercomputers. Namely, for a given channel boundary, we solve Poisson's equation on a grid of points for all required configurations and store the resulting electric potentials and fields in tables. During simulations, the potential and field at any point are calculated by interpolating between the table entries. We show that, using a reasonable number of grid points, it is possible to obtain very accurate estimates of the electric forces. Most importantly, with the speed gained with this method, one can run the computer simulations long enough to determine the conductance of a model channel. Here we present the results of BD simulations of ions in a vestibular channel and discuss the insights these simulations introduce into the ion transport problem.

II. FORMALISM

A. Model of ion channels

Ion channels in biological membranes are formed by a group of four to five proteins, but their precise structure is

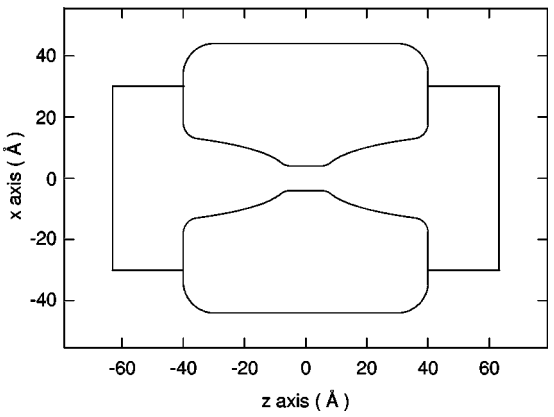

FIG. 1. The model ion channel with two catenary vestibules is generated by rotating the closed curves in the figure along the symmetric z axis by 180°. The vestibules at each side of the membrane are constructed using $z = a \cosh(x/a)$ with $a = 4.87$ Å. The radius of the entrance of the vestibule is 13 Å and the cylindrical transmembrane segment has a radius of 4 Å. The dimensions of the cylindrical reservoirs are 30 Å in radius and 22 Å in height.

not well known yet. Electron microscope pictures of the acetylcholine channel reveal a catenary shape narrowing down to a 4–5 Å radius in the neck region [4]. In modeling the channel boundary, we follow this shape closely (see Fig. 1). For purposes of simulation of ion transport, we place on each side of the vestibules a cylindrical reservoir with a radius of 30 Å and a variable height. The number of ions in each reservoir is fixed for convenience (13 of each species) and the height of the reservoir is adjusted to obtain a desired ionic concentration. The ionic concentration in the volume composed of the channel vestibules and the reservoirs is 300 mM, corresponding to a height of 22 Å. This concentration is about twice that of the physiological concentration and is preferred in the simulations to obtain a better statistics. The cylindrical reservoir has a glass boundary in that an ion moving out of the boundary is reflected back into the reservoir.

An important question in the calculation of the electromagnetic forces is what dielectric constant to use for water inside the channel. Molecular dynamics studies of water in cavities [9] and narrow pores [10] suggest that the dielectric constant is substantially reduced compared to the bulk value. This reduction in ϵ_w clearly depends on the geometry, and in the absence of such a microscopic input for the catenary channel, we prefer to use the bulk value in the present simulations. We note that a smaller value of ϵ_w will lead to a larger image force on an ion and therefore will require a larger dipole strength in the channel neck to cancel this repulsive force and allow permeation of ions (see below).

In earlier studies, charge groups in the protein walls are found to play an important role in ion permeation. To investigate such effects, we place a set of four dipoles inside the protein boundary at $z = 5$ Å and another set of four dipoles at $z = -5$ Å. Their orientations are perpendicular to the z axis. For each dipole, the negative pole, placed at 1 Å inside the water-protein boundary, is separated from the positive pole by 5 Å. Thus, if 5/16 of an elementary charge is placed on each pole, then the total moments of four such dipoles would be 100×10^{-30} C m. The same configuration of dipoles is used in all the simulations, giving rise to an attractive potential for cations and a repulsive potential for anions in the channel. These fixed charges represent the charged side chains thought to form a ring around the entrance of the constricted region [11] and their nearby counter charges. For convenience, we adjust the amount of charge rather than the number or positions of the charges, but in reality the side chains would have one electron charge each. The membrane potential of 100 mV is represented by an applied electric field of strength 10^7 V m^{-1}. This is a simplification we use for convenience. The actual potential and field across the channel are severely distorted by the dielectric boundary [7].

The treatment of water as a continuum is presumably a reasonable approximation in the vestibule of the channel, but it is not expected to work in the narrow neck region. From the point of view of ion transport, the most important effect that cannot be handled by the BD simulations is the dehydration process necessary for an ion to squeeze into the neck region. The loss of water molecules from the first or second hydration shell of an ion will lead to an effective potential barrier that the ion needs to surmount. This intuitive argument is supported by detailed MD studies of the gramicidin pore, which reveal the presence of such an energy barrier at the pore mouth [3]. The temperature dependence of conductance measured in biological ion channels provides additional evidence for an energy barrier: The conductivity-temperature curves in channels are always steeper than those in the bulk electrolyte solutions, which can be explained if one invokes a dynamic energy barrier in the neck region [12]. We model this effect in the BD simulations by erecting potential barriers of height V_B on either side of the channel at $z = \pm 10$ Å. Only those ions that have thermal energies $E > V_B$ are allowed in, otherwise they are elastically scattered from the barrier. The probability of transmission follows from the Boltzmann distribution as

$$\mathcal{P}(E > V_B) = \frac{2}{\sqrt{\pi}} (kT)^{-3/2} \int_{V_B}^{\infty} e^{-E/kT} \sqrt{E}\, dE, \qquad (1)$$

which is given by the incomplete Γ function

$$\mathcal{P}(E > V_B) = \frac{2}{\sqrt{\pi}} \Gamma\left(\frac{3}{2}, \alpha\right) = \frac{2}{\sqrt{\pi}} \exp(-\alpha) \sqrt{\alpha} \times \left(1 + \frac{1}{2\alpha} - \frac{1}{4\alpha^2} + \frac{1}{8\alpha^3} - \cdots\right), \qquad (2)$$

where $\alpha = V_B/kT$. Ideally, this potential barrier should be calculated from the MD simulations and incorporated into the BD algorithm. However, MD studies for general channel shapes are still in their infancy and it is not clear whether one can represent the complex interactions in the neck region with an effective potential acting on the ions only. In the absence of such information, we have used a step barrier for simplicity, but caution that a description of properties such as selectivity may ultimately require switching from BD to MD in the vicinity of the neck region.

B. Brownian dynamics

The trajectories of ions drifting across the channel under the influence of a driving force are followed using BD simulations. The motion of the ith ion with mass m_i and charge q_i is governed by the Langevin equation

$$m_i \frac{d\mathbf{v}_i}{dt} = -m_i \gamma_i \mathbf{v}_i + \mathbf{F}_R(t) + \mathbf{F}_i . \tag{3}$$

The first term on the right-hand side of Eq. (3) corresponds to an average frictional force with the friction coefficient given by $m_i\gamma_i$, where $1/\gamma_i$ is the relaxation time constant of the system. The second term $\mathbf{F}_R(t)$ represents the random part of the collisions and rapidly fluctuates around a zero mean. The frictional and random forces in Eq. (3), together describing the effects of collisions with the surrounding water molecules, are connected through the fluctuation-dissipation theorem [13], which relates the friction coefficient to the autocorrelation function of the random force

$$m_i \gamma_i = \frac{1}{2kT} \int_{-\infty}^{\infty} \langle F_{Ru}(0) F_{Ru}(t) \rangle dt, \quad u = x,y,z, \tag{4}$$

where k and T are the Boltzmann constant and temperature in degrees Kelvin, respectively. Here the angular brackets denote ensemble averages. Finally, $\mathbf{F}_i = q_i \mathbf{E}_i$ in Eq. (3) denotes the total electric force acting on the ion. The electric field $\mathbf{E}_i$ arises from (i) other ions, (ii) fixed charges in the protein, (iii) membrane potential, and (iv) induced surface charges on the water-protein boundary. It is computed by solving Poisson's equation and will be further discussed in Sec. II C.

The solution of the Langevin equation is implemented using the third-order BD algorithm proposed by van Gunsteren and Berendsen [14,15]. The main steps of the solution needed in this implementation are given in the Appendix. Unlike many other BD algorithms, the time steps Δt in this algorithm are not restricted by the condition $\Delta t \ll \gamma^{-1}$. For typical ions (Na or K), this condition would have required $\Delta t \sim 1$ fs, thus making the long-time simulations needed to obtain the macroscopic current virtually impossible. The physical constraints of the ion channel, on the other hand, impose a much more relaxed time step. For example, keeping the rate of change of the electric field in the channel to a few percent requires $\Delta t = 100$ fs, which is used in the following BD simulations. The basic computational steps of the algorithm are as follows.

(i) Compute the electric force $\mathbf{F}(t_n) = q_i \mathbf{E}_i$ acting on the ion i at time t_n from the lookup table and calculate its derivative $[\mathbf{F}(t_n) - \mathbf{F}(t_{n-1})]/\Delta t$.

(ii) Compute a net stochastic force impinging on an ion over the time period of Δt from a sampled value of $\mathbf{F}_R(t)$.

(iii) Determine the position of each ion at time $t_n + \Delta t$ and its velocity at time t_n by substituting $\mathbf{F}(t_n)$, its derivative $\dot{\mathbf{F}}(t_n)$, and $\mathbf{F}_R(t)$ into the solutions of the Langevin equation, Eqs. (A6) and (A7).

(iv) Repeat the above steps for all ions in the system for a desired number of simulation steps.

The BD program used in the simulations is written in FORTRAN, vectorized, and executed on a supercomputer (Fujitsu VPP-300). A typical simulation is run for 2 000 000 steps, which is repeated 5 times. With 52 ions in the reservoirs, the CPU time of a supercomputer needed to complete one simulation period of 0.1 μs (10^6 time steps in 100 fs) is about 2 h. The current is determined from the total number of ions crossing the transmembrane segment. To ensure that the desired intracellular and extracellular ion concentrations are maintained throughout the simulation, a stochastic boundary is applied. When an ion crosses the transmembrane segment, an ion of the same species from the same side is transplanted on the opposite side.

The following physical constants are employed in the BD simulations: dielectric constants $\epsilon_{\text{water}} = 80$ and $\epsilon_{\text{prot}} = 2$; masses $m_{\text{Na}} = 3.8 \times 10^{-26}$ kg and $m_{\text{Cl}} = 5.9 \times 10^{-26}$ kg; diffusion coefficients $D_{\text{Na}} = 1.33 \times 10^{-9}$ m^2 s^{-1} and $D_{\text{Cl}} = 2.03 \times 10^{-9}$ m^2 s^{-1}; relaxation time constants γ^{-1}, $\gamma_{\text{Na}} = 8.1 \times 10^{13}$ s^{-1} and $\gamma_{\text{Cl}} = 3.4 \times 10^{13}$ s^{-1}; ion radii $r_{\text{Na}} = 0.95$ Å and $r_{\text{Cl}} = 1.81$ Å; and room temperature $T_r = 298$ K.

C. Lookup tables for electric forces

The BD algorithm requires calculation of electric forces acting on ions at each time step. Given the positions of ions, this can be achieved by solving Poisson's equation in an appropriate boundary. However, as emphasized in the Introduction, this direct approach is computationally too expensive to be useful in long-time simulations necessary for the calculation of conductance. Here we adapt an alternative method where the electric field and potential are precalculated on a grid of points for various configurations and the results are stored in a number of lookup tables. During simulations, the field and potential at desired points are reconstructed by interpolating between the table entries. Compared to the analytical solution of Poisson's equation in toroidal coordinates, the lookup method is two orders of magnitude faster. The lookup method has the additional advantage that one is not restricted to a toroidal channel. Numerical solutions of Poisson's equation for more realistic channel shapes (e.g., catenary) can be as easily stored in tables as is done in the present work.

For calculational purposes, it is convenient to break the total electric potential V_i experienced by an ion i into four pieces

$$V_i = V_{S,i} + V_{X,i} + \sum_{j \neq i} V_{I,ij} + \sum_{j \neq i} V_{C,ij}, \tag{5}$$

where $V_{S,i}$ is the self-potential due to the surface charges induced by the ion i on the channel boundary and $V_{X,i}$ is the external potential due to the applied field, fixed charges in the protein wall, and charges induced by these. The next two terms in Eq. (5) take the influence of other ions into account, namely, $V_{I,ij}$ is the image potential due to the charges induced by the ion j and $V_{C,ij}$ is the Coulomb potential due to the ion j, which is computed directly from

$$V_{C,ij}=\frac{1}{4\pi\epsilon_0}\frac{q_j}{\epsilon_w|\mathbf{r}_i-\mathbf{r}_j|}, \tag{6}$$

where $\mathbf{r}_i$ and $\mathbf{r}_j$ are the positions of the ions. The electric field experienced by the ion is decomposed in the same way

$$\mathbf{E}_i=\mathbf{E}_{S,i}+\mathbf{E}_{X,i}+\sum_{j\neq i}\mathbf{E}_{I,ij}+\sum_{j\neq i}\mathbf{E}_{C,ij}, \tag{7}$$

each field component being defined as in the potential (5).

The first three components in Eqs. (5) and (7) depend on the boundary and, in general, they are determined from numerical solutions of Poisson's equation (see Refs. [5,6] for iterative techniques of solution). Each of these components is calculated for a grid of positions and stored in separate tables. To allow rapid look up, the precalculated values must be on an evenly spaced grid. Because the use of a rectilinear grid would result in many wasted points and a jagged edge near the pore boundary, we use a system of generalized cylindrical coordinates in constructing the look up tables. In terms of the cylindrical coordinates (r,θ,z)

$$r=\sqrt{x^2+y^2},\quad \theta=\tan^{-1}(y/x),\quad z=z, \tag{8}$$

the generalized coordinates (ρ,θ,ζ) are defined as

$$\rho(r,z)=r/r_{\max}(z),\quad \theta=\theta,\quad \zeta(z)=(z-z_{\min})/(z_{\max}-z_{\min}), \tag{9}$$

where $r_{\max}(z)$ is the limiting radius of the pore and $z_{\max}$ and $z_{\min}$ are the maximum and minimum z coordinates for the system. The coordinates ζ and ρ are normalized and cover the range $[0,1]$. For θ, we use the range $[-\pi,\pi]$ for convenience (see below). The limiting radius $r_{\max}(z)$ is offset from the pore wall by the radius of the smallest ion in the simulation, which defines the closest possible approach for an ion to the pore wall. Besides providing a smooth edge near the boundary, the generalized coordinates also allow the cylindrical symmetry of the channel to be exploited. For example, the θ coordinate is redundant in the calculation of the self-potential $V_{S,i}$, therefore it is stored in a two-dimensional table $V_{2D}(\rho_m,\zeta_n)$. Similarly, the image potential $V_{I,ij}$ depends on the relative angle between the ions i and j and it is stored in a five-dimensional table $V_{5D}(\rho_m,\zeta_n,\rho_{m'},\zeta_{n'},\theta_k)$. Due to reflection symmetry, θ_k and $-\theta_k$ lead to the same image potential. Hence θ_k in V_{5D} covers only the range $[0,\pi]$. The fixed charges do not possess any particular symmetry, so the external potential $V_{X,i}$ is stored in a full three-dimensional table $V_{3D}(\rho_m,\zeta_n,\theta_k)$. Here θ_k covers the whole range $[-\pi,\pi]$.

The electric field is stored in the same way as the potential, except that three values are required for each point in a table, one for each Cartesian component of the field. So while the field tables are indexed by the generalized coordinates, their contents are stored as Cartesian coordinates in the tables $\mathbf{E}_{2D}(\rho_m,\zeta_n)$, $\mathbf{E}_{3D}(\rho_m,\zeta_n,\theta_k)$, and $\mathbf{E}_{5D}(\rho_m,\zeta_n,\rho_{m'},\zeta_{n'},\theta_k)$. Note that, in principle, these results could be combined and stored in the same table. However, separate tables are more flexible and assist in minimizing the interpolation error, and therefore preferred.

During the simulations, first the positions of ions at a given time step are converted to the generalized coordinates. The values of the electric potential and field at the position of the ion are then extracted from the tables by multidimensional linear interpolation, making use of a simple algorithm that generalizes easily to dimensions greater than 2 [16]. Because the grid points are evenly spaced in the generalized coordinates, the appropriate indices can be found by division rather than by a time consuming binary search. For an ion i with charge q_i at the position $\mathbf{r}_i=(\rho_i,\zeta_i,\theta_i)$ and another ion with charge q_j at $\mathbf{r}_j=(\rho_j,\zeta_j,\theta_i)$, the potentials are given by

$$\begin{aligned} V_{S,i}&=\frac{q_i}{e}V_{2D}(\rho_i,\zeta_i),\\ V_{X,i}&=V_{3D}(\rho_i,\zeta_i,\theta_i),\\ V_{I,ij}&=\frac{q_j}{e}V_{5D}(\rho_i,\zeta_i,\rho_j,\zeta_j,|\theta_i-\theta_j|), \end{aligned} \tag{10}$$

where $V_{2D}(\rho_i,\zeta_i)$, $V_{3D}(\rho_i,\zeta_i,\theta_i)$, and $V_{5D}(\rho_i,\zeta_i,\rho_j,\zeta_j,|\theta_i-\theta_j|)$ are obtained by applying the interpolation algorithm to the two-dimensional self-potential table, the three-dimensional external potential table, and the five-dimensional image potential table, respectively. The self-potential and image potential tables are constructed assuming a positive unit charge as the source, so the results are rescaled to the actual source charge after lookup.

The symmetries used to reduce the size of the tables require that the recovered electric field be rotated and reflected appropriately so that it corresponds to the simulation's Cartesian axes. The fields are extracted from the interpolated table values as

$$\begin{aligned} \mathbf{E}_{S,i}&=\frac{q_i}{e}R_z(\theta_i)\mathbf{E}_{2D}(\rho_i,\zeta_i),\\ \mathbf{E}_{X,i}&=\mathbf{E}_{3D}(\rho_i,\zeta_i,\theta_i),\\ \mathbf{E}_{I,ij}&=\frac{q_j}{e}\mathcal{R}_y(\theta_i,\theta_j)R_z(\theta_i)\mathbf{E}_{5D}(\rho_i,\zeta_i,\rho_j,\zeta_j,|\theta_i-\theta_j|), \end{aligned} \tag{11}$$

where $R_z(\theta_i)$ denotes the rotation matrix around the z axis by an angle θ_i and $\mathcal{R}_y(\theta_i,\theta_j)$ is a reflection operator on the x-z plane defined by

$$\mathcal{R}_y(\theta_i,\theta_j)=\begin{cases} D(1,1,1) & \text{if}\quad \pi>\theta_j-\theta_i>0\\ D(1,-1,1) & \text{if}\quad 0>\theta_j-\theta_i>-\pi. \end{cases} \tag{12}$$

Here D denotes a diagonal matrix with entries as indicated in the arguments.

Once the field and potential are known, the force and potential energy on ion i can be calculated from

$$\mathbf{F}_i=q_i\mathbf{E}_i, \tag{13}$$

$$U_i=q_i(V_i-\tfrac{1}{2}V_{S,i}). \tag{14}$$

Note that only half the self-potential is used when calculating the potential energy. The reason for this can be seen by imagining the charge on the ion being built up with infinitesimal pieces being brought in from infinity. While the external potential remains the same during this process, the self-potential increases from zero to its full value as the charge is built up. This involves the integral $\int_0^{q_i} q\, dq = q_i^2/2$, which explains the factor of one-half.

To test the accuracy of the lookup method, we compare the interpolation results for potential energy and force with those obtained from the analytical solution of Poisson's equation for a toroidal channel in a variety of situations. The channel boundary is generated by rotating a circle in the x-z plane around the z axis. The radius of the circle is 40 Å and its center is located at $x=44$ Å, $z=0$. We refer to Ref. [7] for details of the analytical solution. The results of electric potential and each Cartesian component of the field for the self-, external, and image parts are stored in tables with dimensions 37×97, $10\times171\times40$, and $7\times119\times7\times119\times14$, respectively. These dimensions are found after an optimization of the lookup program for the toroidal channel. The catenary channel described in Fig. 1 has a similar shape and lookup tables with the same dimensions are used in the BD simulations in Sec. III.

Among the three potential (or field) parts, the self-potential displays larger errors compared to the image and external potentials. Therefore, in the following tests, we focus on the potential energy and the force on a single ion in a toroidal channel that has no other fixed charges or external fields. In Fig. 2 we show the potential energy and the z component of the force for a single ion moving parallel to the central axis but offset from it by 3 Å. Since the z component of the force provides the driving force in the BD simulations, only that one is shown in this figure. The solid lines are calculated from the analytical method and the circles by interpolating from the precalculated values stored in the lookup tables. The spacing between points in the lookup table is 1.77 Å in the z direction and the circles are at the midpoints of these intervals, where the maximum interpolation error is expected to occur. The radius of the channel varies with z and hence the spacing between points in the r direction changes. Therefore, the circles are not necessarily located at the midpoints of the interpolation intervals in the radial direction. The relative error for the potential and force are not shown in a separate graph because they are less than 1% for all the points in Fig. 2. Almost identical results are obtained for other ion trajectories parallel to the central axis, but with different radial offsets. In Fig. 3 we show a similar plot of the potential energy and the radial component of the force in the $z=0$ plane as the ion is moved radially from the central axis towards the boundary. Note that the closest approach is limited by the size of the ion. Here the circles correspond to the midpoints of the interpolation intervals in both the z and the radial directions. The relative error is again less than 1% for all the points in Fig. 3. In Fig. 4 we show another comparison for the potential energy and the radial component of the force on a radial trajectory in the $z=30$ Å plane. Again the circles are chosen at the midpoints of the interpolation intervals. The relative error remains less than 1% for the potential, but rises to a few percent for the force for points near the boundary in Fig. 4. The agreement between the analytic and lookup methods evident in Figs. 2–4 indicates that the interpolation error is negligible for the potential energy and the force in the most important parts of the channel.

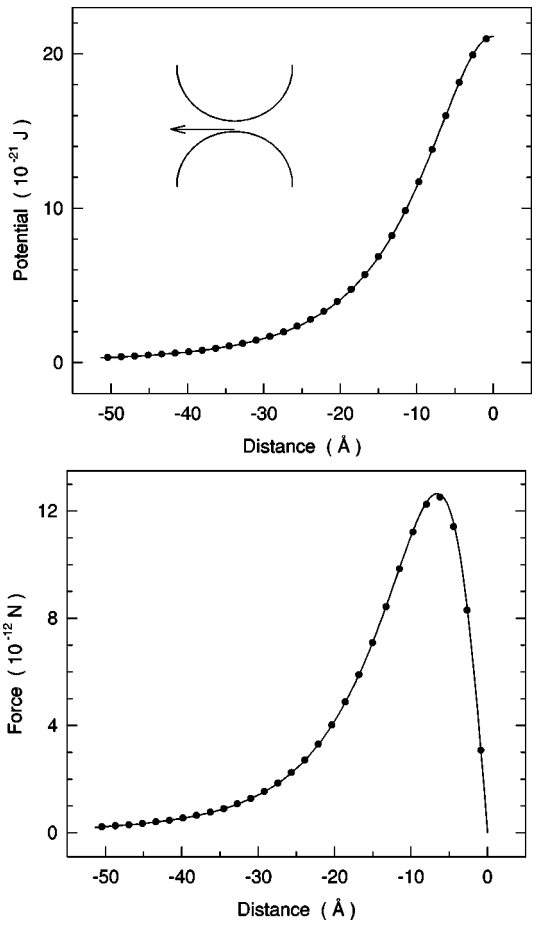

FIG. 2. Comparison of the potential energy and the z component of force, obtained from the lookup tables by interpolation (circles), with the analytical solutions (lines) for a toroidal channel. An ion is moved along the trajectory that is parallel to the central axis but is offset from it by 3 Å, as indicated by the arrow in the inset. The position of each circle in the z direction is located at the midpoint between two adjacent points stored in the lookup table.

Tests carried out on a catenary channel yield a similar agreement between the lookup method and the numerical solution results. The relative error is slightly larger when an ion approaches the vestibular wall in the catenary channel, but this is not of great concern in simulations since ions tend to stay away from the water-protein boundary.

The system of generalized coordinates we use has a weakness at the entrance to the pore, where the boundary runs horizontally, perpendicular to the z axis. The radius suddenly jumps from that of the reservoir to that of the pore entrance. This results in spurious interpolation between points near the channel's top surface and points in the pore entrance. Errors in the potential near the channel's top surface are unlikely to affect the results of simulations. Errors in the potential in the pore entrance are of greater concern. However, the magnitude of the force is rather small in this region and we have

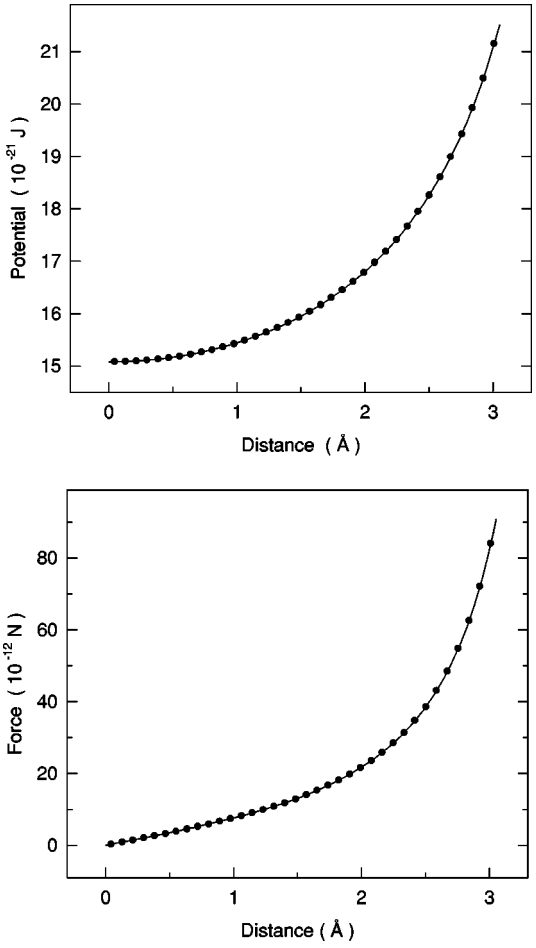

FIG. 3. Same as Fig. 2, but for a radial trajectory in the $z=0$ plane and the radial component of the force. The lookup results (circles) are calculated at the midpoints of the interpolation intervals in both the z and the radial directions.

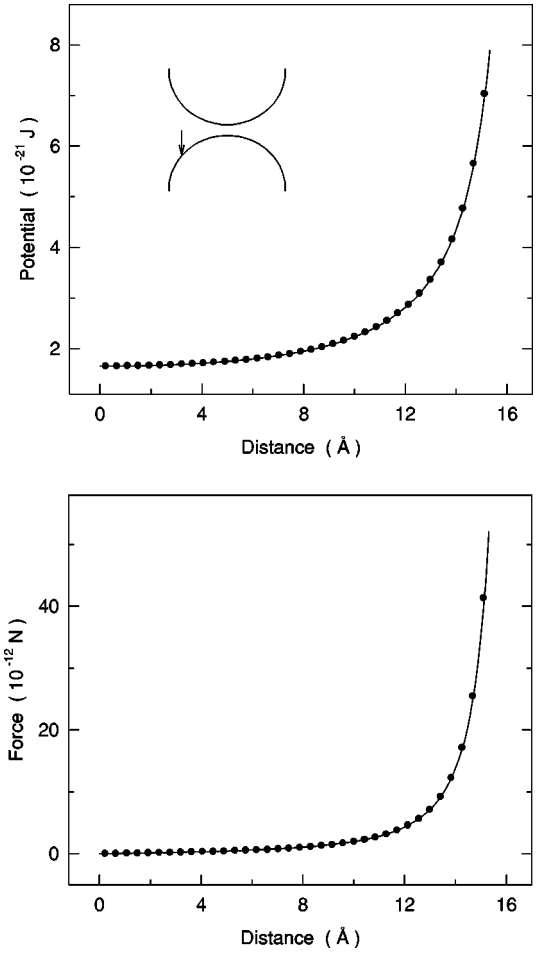

FIG. 4. Same as Fig. 3 but for a radial trajectory in the $z=30$ Å plane (see the inset).

checked in control runs that it has no effect on the simulations. An improved system of generalized coordinates that avoids this problem may be desirable in other applications of this method.

The use of lookup tables is practical despite the large number of points at which the field needs to be calculated because the time used by the algorithms depends much more on the number of solutions needed rather than the number of points per solution. Both the iterative and analytical algorithms can easily generate the field at multiple points arising from many charges at given positions (which we call one solution). On the VPP, a solution for 50 ions and 16 fixed charges takes 0.3 s (of CPU time) by the analytical algorithm, 6 s by the iterative algorithm, but only 0.005 s by the lookup table method. A BD simulation of 2×10^6 steps would thus take (including overheads) 170 h by the analytical algorithm, 140 d by the iterative method, and 4 h by the lookup table method. The filling of the tables takes only 1 h using the analytical solution and 10 h using the iterative solution. To give an example, generating a five-dimensional lookup table using the iterative method (which is the most time consuming) requires only 833 solutions, each for a single ion and at 12 000 points. Each solution takes 21 s and the total time required is about 5 h. Another advantage of the method is that once the tables are constructed for a given geometry, they can be used in many simulations studying different aspects of channel conductance.

III. BROWNIAN DYNAMICS SIMULATIONS OF CONDUCTANCE

Previously, we used the BD simulations to study trajectories of ions in a toroidal channel [8]. The main conclusions of that work are (i) the repulsive self-potential of an ion is strong enough to make the channel impermeable even in the presence of an applied electric potential of 100 mV and (ii) dipoles of a favorable orientation are required to cancel this repulsive force and make the channel permeable. The use of lookup tables allows much longer simulation times, which we exploit here to study the conductance of the model catenary channel described in Sec. II A. In particular, we consider the effect of the potential barrier on the channel conductance. In Fig. 5 we show the current-voltage relationship obtained in five different simulations as the barrier height takes the values $V_B=0,\ 3,\ 4,\ 5,$ and $6\ \ kT_{\rm r}$. The results for $V_B=1$ and $2\ \ kT_{\rm r}$ are not shown to avoid cluttering ($1kT_{\rm r}$ overlaps with $0\ \ kT_{\rm r}$ and $2\ \ kT_{\rm r}$ is slightly suppressed with respect to $0\ \ kT_{\rm r}$ but retains its linear character). The outstanding feature of these curves is the increasing deviation from the linear Ohm's law as the barrier height increases. The curvature mostly occurs in the region $eV\sim V_B$ and one

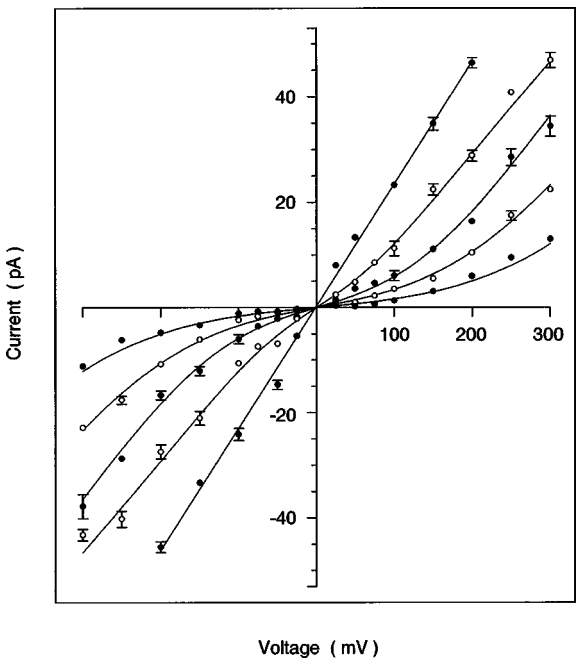

FIG. 5. Evolution of the current-voltage relationships with the barrier height for symmetrical solutions. Current flowing across the channel is measured at different applied potentials. The data points are fitted with a modified Ohm law, which takes the barrier into account [see Eq. (15)].

recovers the linear I-V curves at the asymptotic regions albeit with different conductances. Intuitively, the relative suppression of the current at low voltages follows from the fact that the potential barrier is most effective when the driving force is small. These observations suggest a modification of Ohm's law with a Pöschl-Teller function [17]

$$I=\frac{\gamma V}{1+\beta/\cosh\,(eV/V_B)}, \tag{15}$$

where γ is the limiting conductance and β is a dimensionless constant. When $eV\gg V_B$, the denominator goes to 1 and one recovers Ohm's law. For $eV\ll V_B$, Eq. (15) is again linear but with a conductance reduced to $\gamma/(1+\beta.)$ The nonlinearities in the I-V curves become apparent only when $eV\sim V_B$, which corresponds to the region $V\approx 100-200$ mV for the above barriers. The lines in Fig. 5 are obtained by fitting Eq. (15) to the I-V data. The fit values of the parameters γ and β are given in Table I. While Eq. (15) does a good job of describing the data for a given barrier, variation of the fit parameters with V_B indicates that it is too simplistic to give a consistent picture for all the data in Fig. 5. For example, the rapid change in β implies a faster suppression of the current with increasing barrier than envisioned in Eq. (15). We have not attempted a global fit of the data since it appears unlikely that the complexities of the BD simulations could be summarized in a simple, single formula.

TABLE I. Values of the parameters γ and β in Eq. (15) obtained from fits to the I-V data in Fig. 5.

$V_B(kT_r)$	γ (pS)	β
0	232 ± 4	
3	159 ± 4	0.63 ± 0.18
4	151 ± 7	2.44 ± 0.41
5	130 ± 11	3.74 ± 0.68
6	138 ± 80	9.12 ± 7.02

For symmetrical solutions, the current-voltage relationship obtained from patch-clamp recordings is usually Ohmic. (Here we are not concerned with nonlinearities that arise from rectification.) These measurements are typically carried out with the applied voltage in the biological range 0–100 mV. The BD simulations presented above suggest that the current-voltage relations would deviate from straight lines if there are potential barriers in the channel, but the deviation would be apparent only at higher values of the applied voltage (100–200 mV). There are already some experimental indications for a deviation from Ohm's law [18]. It would be worthwhile to pursue this question further in future patch-clamp experiments where the applied voltage is pushed beyond the usual range. If such deviations do occur, fitting the data points with Eq. (15) will provide an estimate of the barrier height present in the channel.

IV. CONCLUSIONS

Electric forces play an important role in ion transport across membrane channels and therefore they form an essential part of any model channel. In this paper we proposed a lookup method for calculation of electric forces, which enables computer simulation studies of ion conductance to be carried out for biological channels with vestibular shapes. As demonstrated in Sec. II, the method is fast, accurate, and allows arbitrary shapes of channels. As an application of the method, we have performed Brownian dynamics simulations of ion conductance in a model catenary channel. The results highlight the role played by potential barriers in channel dynamics and how they could explain deviations in current-voltage relations from Ohm's law. Conversely, the observation of nonlinearities in patch-clamp experiments would shed light on the presence and nature of potential barriers in biological channels. Such effects should be actively pursued in future patch-clamp experiments where the applied voltage is pushed beyond the usual biological range.

APPENDIX: SOLUTION OF LANGEVIN EQUATION

Here we give the basic steps in the solution of the Langevin equation that are implemented in the BD algorithm of van Gunsteren and Berendsen [15]. Using the the integrating factor $e^{\gamma t}$, the Langevin equation (3) can be integrated from an initial time t_n to t to obtain for the velocity

$$v(t)\;e^{\gamma t}-v(t_n)\;e^{\gamma t_n}=\frac{1}{m}\int_{t_n}^{t}[F(t')+F_R(t')]\;e^{\gamma t'}dt'. \tag{A1}$$

Here and in the following the indices referring to ions and Cartesian components are omitted for convenience. The integral over the random force in Eq. (A1) can be obtained using the stochastic properties of $F_R(t)$. For the electric force, we Taylor expand $F(t)$ around t_n,

$$F(t)=F(t_n)+\dot{F}(t_n)(t-t_n)+\cdots, \tag{A2}$$

where $\dot{F}(t_n)$ denotes the derivative $F(t)$ at $t=t_n$. Here the first-order expansion of $F(t)$ is sufficient as the positions in the BD algorithm are exact to third order. Substituting Eq. (A2) in Eq. (A1) and integrating the force terms gives

$$v(t)=v(t_n)\ e^{-\gamma(t-t_n)}+\frac{F(t_n)}{m\gamma}(1-e^{-\gamma(t-t_n)}) + \frac{\dot{F}(t_n)}{m\gamma^2}[\gamma(t-t_n)-1+e^{-\gamma(t-t_n)}] + \frac{e^{-\gamma t}}{m}\int_{t_n}^{t} F_R(t')\ e^{\gamma t'}dt'. \quad \text{(A3)}$$

To find the position after a time step Δt, we need to integrate Eq. (A3) once more from t_n to $t_n+\Delta t$. Integration of all the terms in Eq. (A3) is straightforward, except the last one, which can be done by parts using $du=e^{-\gamma t}$ and v as the integral of F_R,

$$\int_{t_n}^{t_n+\Delta t}\frac{e^{-\gamma t}}{m}\int_{t_n}^{t} F_R(t')\ e^{\gamma t'}dt' = \frac{1}{m\gamma}\int_{t_n}^{t_n+\Delta t}[1-e^{\gamma(t-t_n-\Delta t)}]F_R(t)dt \equiv X_n(\Delta t), \quad \text{(A4)}$$

where we have defined the random variable $X_n(\Delta t)$, which has the same stochastic properties as $F_R(t)$. We refer to Ref. [15] for details of how $X_n(\Delta t)$ is implemented in the BD algorithm. Using Eq. (A4), the position at time $t_{n+1}=t_n+\Delta t$ is found to be

$$x(t_{n+1})=x(t_n)+\frac{v(t_n)}{\gamma}(1-e^{-\tau})+\frac{F(t_n)}{m\gamma^2}(\tau-1+e^{-\tau}) + \frac{\dot{F}(t_n)}{m\gamma^3}\left(\frac{\tau^2}{2}-\tau+1-e^{-\tau}\right)+X_n(\Delta t). \quad \text{(A5)}$$

Here $\tau=\gamma\Delta t$ is a dimensionless parameter that signifies a diffusive regime when $\tau\gg 1$ or a microscopic one when $\tau \ll 1$. A more convenient form for $x(t_{n+1})$, which does not involve the velocity, can be obtained by adding $e^{-\tau}$ times $x(t_{n-1})\equiv x(t_n-\Delta t)$ to Eq. (A5),

$$x(t_{n+1})=x(t_n)(1+e^{-\tau})-x(t_{n-1})e^{-\tau}+\frac{F(t_n)}{m\gamma^2}\tau(1-e^{-\tau}) + \frac{\dot{F}(t_n)}{m\gamma^3}\left(\frac{\tau^2}{2}(1+e^{-\tau})-\tau(1-e^{-\tau})\right)+X_n(\Delta t) - X_n(-\Delta t)e^{-\tau}. \quad \text{(A6)}$$

Similarly, a simple expression for the velocity follows by subtracting $x(t_{n-1})$ from Eq. (A5),

$$v(t_n)=\frac{2\gamma}{\sinh\tau}\left[x(t_{n+1})-x(t_{n-1})+2\left(\frac{F(t_n)}{m\gamma^2}-\frac{\dot{F}(t_n)}{m\gamma^3}\right) \times(\sinh\tau-\tau)-X_n(\Delta t)+X_n(-\Delta t)\right]. \quad \text{(A7)}$$

Equations (A6) and (A7) provide the basic input for the BD algorithm used in the simulations.

[1] B. Hille, *Ionic Channels of Excitable Membranes* (Sinauer, Sunderland, MA, 1992).
[2] K. Cooper, E. Jakobsson, and P. Wolynes, Prog. Biophys. Mol. Biol. **46**, 51 (1985).
[3] B. Roux and M. Karplus, Annu. Rev. Biophys. Biomol. Struct. **23**, 731 (1994).
[4] C. Toyoshima and N. Unwin, Nature (London) **336**, 247 (1988).
[5] D.G. Levitt, Biophys. J. **22**, 209 (1978).
[6] M. Hoyles, S. Kuyucak, and S.H. Chung, Biophys. J. **70**, 1628 (1996).
[7] S. Kuyucak, M. Hoyles, and S.H. Chung, Biophys. J. **74**, 22 (1998).
[8] S.C. Li, M. Hoyles, S. Kuyucak, and S.H. Chung, Biophys. J. **74**, 37 (1998).
[9] L. Zhang, H.T. Davis, D.M. Kroll, and H.S. White, J. Chem. Phys. **99**, 2878 (1995).
[10] M.S.P. Sansom, G.R. Smith, C. Adcock, and P.C. Biggin, Biophys. J. **73**, 2404 (1997).
[11] N. Unwin, Neuron **3**, 665 (1989).
[12] S. Kuyucak and S.H. Chung, Biophys. Chem. **52**, 15 (1994); S.H. Chung and S. Kuyucak, Neurosci. Lett. **187**, 181 (1995).
[13] F. Reif, *Fundamentals of Statistical and Thermal Physics* (McGraw-Hill, New York, 1965).
[14] W.F. van Gunsteren, H.J.C. Berendsen, and J.A. Rullmann, Mol. Phys. **44**, 69 (1981).
[15] W.F. van Gunsteren and H.J.C. Berendsen, Mol. Phys. **45**, 637 (1982).
[16] W.H. Press, B.P. Flannery, S.A. Teukolsky, and W.T. Vetterling, *Numerical Recipes* (Cambridge University Press, New York, 1992).
[17] G. Pöschl and E. Teller, Z. Phys. **83**, 143 (1933).
[18] S.D. Tyerman, B.R. Terry, and G.P. Findlay, Biophys. J. **61**, 736 (1992).